RESEARCH ACTIVITIES III
Department of Electronic Structure

III-A Synthesis and Characterization of Exotic Molecule Based Nano-Crystals with Transition Metal Cations : Toward Electron Beam Writing Yielding Metal Dot Arrays and Wires Encapsulated in Carbon Shells

Observation of photoelectron and vibrational spectra of gaseous M–C_2 molecules and clusters, where M = Fe, Co, Ni *etc.*, reminds us high potentiality of these salt-type clusters and nano-crystals for magnetic, catalytic and electronic functionalities. Due to the instability of the carbide compounds, the characterization of the MC_2 compounds has been left unknown. We have found that including MnC_2, all transition metal C_2 salt crystals are ferromagnetic, and that M^{2+}–C_2^{2-} ionic nano-crystals are the best materials for generating nano-metals encapsulated in carbon shells. Annealing or heating above 300 °C induces reduction of cations by anions and resulting segregation of metal atoms by locating C_2 radicals outer and connecting C_2 bi-radicals as graphite-like carbon shells. The relatively low segregation temperatures for FeC_2 and NiC_2 make it possible to draw metallic dots or wire circuits in MC_2 thin layers by scanning electron or laser beams. The small size matrix MC_2 crystals prevent the strong dipole-dipole interaction between the metallic dots, while one can also wash out the matrix salt crystals by acid solution leaving the carbon encapsulated nano-metals on the base plate.

III-A-1 Formation of Air-Stable Fe Nano-Particles in Polar Organic Solution: Fe Nano-Crystals with Graphitic Skin 3.5 nm Thick

KOSUGI, Kentaroh; BUSHIRI, Junaid M. ; NISHI, Nobuyuki

[*Appl. Phys. Lett.* in press]

In the process of investigating formation and characterization of FeC_2 nano-crystals, we found that $Fe^{2+}C_2^{2-}$ salt crystals are ferromagnetic and converted to neutral α-Fe nano-particles encapsulated in graphite-like carbon shells. The thickness of the carbon shells is almost constantly 3.5 nm without regard to size and shape, and corresponds to 10 layers of the graphite sheet, although the shells exhibit curvatures and straight lines bound to the metal core surfaces.

Fine particles of CaC_2 are suspended in acetonitrile solution of $FeCl_2$ and heated in a Pyrex tube situated in a pressure-resistant stainless steel vessel at 250 ºC for 48 hrs. The solution was stirred for the first 4 hrs. but the stirring was stopped the other 20 hrs. The solids obtained on the bottom of the tube contained organic compounds produced by the catalytic reacton of the intermediate product, FeC_2. The black magnetic particles are collected by magnets attached on the side wall of an Erlenmeyer flask and washed by methanol in a ultrasonic cleaning bath three times. Transmission electron microscope (TEM) images of the black deposit are shown in Figure 1. The powder was fixed in an epoxi-resin and sliced to a thickness of approximately 60 nm by a Leica Ultracut UCT microtome. X-ray diffraction pattern of the black deposit was displayed in Figure 2. From the width of α-carbon signals, the average size of the Fe cores is estimated to be 60 nm. At 2θ = 26.0°, a broad signal with asymmetric shape is seen. Bulk graphite shows a sharp peak at 2θ = 26.5°. It is reasonable that we see a peak slightly shifted to lower angle and a wide width correspondent with 3.5 nm thickness. TEM images in Figure 1 clearly show that the thickness of the carbon shells with various shapes and sizes are always 3.5 nm.

In principle, the thermal segregation of FeC_2 should produce Fe and carbon in 1:2 molar ratio. In the TEM observation, we saw amorphous carbon and the metallic Fe particles encapsulated in the carbon shells. The constant thickness of the graphite-like shells suggests the presence of attractive field on the metal core surface. This field must be produced by surface Fe atoms, and thus dependent only on the distance from each surface atom. The size of the particle is not concerned with the field generation. The surface Fe atoms are seen to be in good contact with the shell carbon atoms innermost. This contact may be due to ionic interaction remained only on the surface and the charge separation stabilized by occupation of an excess electron, originally in the carbon shell, in a Rydberg orbital of the cationic Fe atom. This hypothesis can be checked by examining other M(transition metal)C_2 compounds.

In the lower part, a TEM image of Fe-wire encapsulating carbon nano-tube (multi-wall) and an expanded image of its boader area are shown.

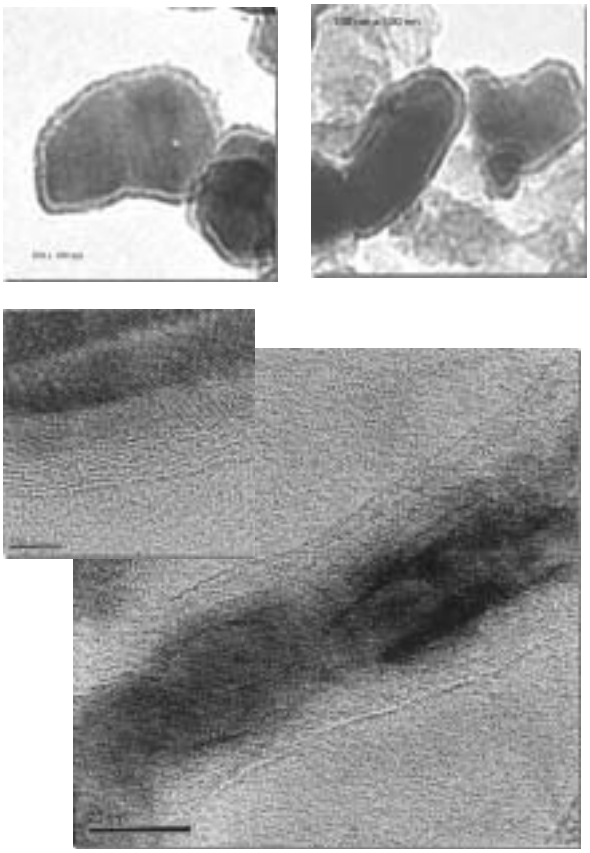

Figure 1. TEM images of α-Fe metallic nano-particles encapsulated in carbon-shell 3.5 nm thick (top) and Fe-wire encapsulating carbon nano-tube(lower).

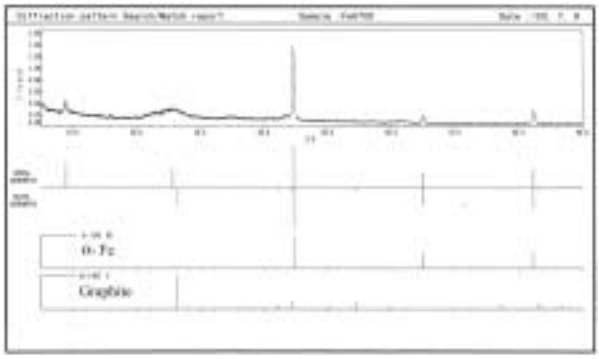

Figure 2. X-ray diffraction pattern of the Fe nano-metals encapsulated in graphite-like carbon shells 3.5 nm thick.

III-A-2 Infrared Absorption Studies of M(transition metal)$^{2+}C_2^{2-}$ Compounds: Bonding Nature and their Stabilities

BUSHIRI, Junaid M. ; KOSUGI, Kentaroh; HINO, Kazuyuki; NISHI, Nobuyuki

Transition metal C_2 compounds have been believed to be non-existent materials. In fact, as far as the metallic part is neutral, the presence of MC_2 is hardly possible due to the inequivalency of the bonding nature of M and C_2. Since C_2 is a di-valent anion, C_2^{2-}, on the other hand, a rock-salt type compound $M^{2+}C_2^{2-}$ can be stabilized by ionic interaction between cations and anions just like CaC_2 and MgC_2. For the synthesis, the simple ion exchange reaction is expected to produce MC_2 salts.

Since CaC_2 reacts with water producing acetylene (C_2H_2) and $Ca(OH)_2$, MCl_2 salt compounds are dissolved in dehydrated acetonitrile. In this solution, fine powders of CaC_2 are suspended and stirred gently. At the temperatures lower than 70 ºC, nothing happens in the solution. At above 75 ºC, the black precipitates are accumulated on the bottom of the reaction vessel.

Figure 1 displays the IR spectra of various ionic MC_2 compounds (M = Ca^{2+}, Mn^{2+}, Fe^{2+}, Co^{2+}, and Ni^{2+}. The doubly degenerated C=C stretching vibration bands of $Ca^{2+}C_2^{2-}$ are seen at 1418 and 1488 cm^{-1}. Among 6 coordinated C_2^{2-} ions, the four C_2^{2-} are located equivalently around the Ca^{2+} ion in a tetrahedral crystal of CaC_2. For one antisymmetric combination of the two C=C stretching oscillators, two sets of symmetric and anti-symmetric oscillators in other two axes split into low energy components and high energy components depending upon in-line (–C=C–Ca–C=C–) configuration or in-parallel configuration of the two C_2 oscillators. Thus the doublet appears around 1450 cm^{-1}. This splitting becomes much narrower in NiC_2.

The Fe–C stretching vibration in the gas phase FeC_2 molecule was found to be 550 cm^{-1} by ZEKE photo-electron spectroscopy (Drechsler *et al., J. Mol. Struct.* **348**, 337 (1995)). In the nano-crystals, a peak of a very broad band is seen at 456 cm^{-1}. The spectral feature of this band is similar to that of MnC_2, while those of CoC_2 and NiC_2 shift to much high frequencies around 600 cm^{-1}. Thus one can see that the M–C bonds in CoC_2 and NiC_2 is strong while those in MnC_2 and FeC_2 are rather weaker. This is in consistent with the reactivity of MC_2 compounds with water. CoC_2 and NiC_2 are stable against water, but MnC_2 and FeC_2 are reactive with water.

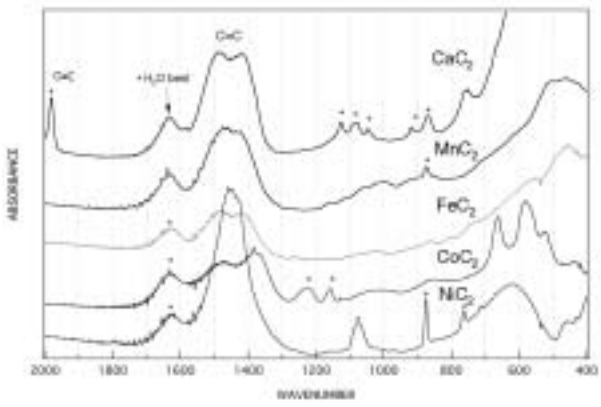

Figure 1. IR Spectra of MC_2 compounds.

III-A-3 Magnetic Behavior of MnC_2 and NiC_2

BUSHIRI, Junaid M.; KOSUGI, Kentaroh; NISHI, Nobuyuki

Most of manganese compounds, such as MnO, MnO_2, MnS, and $MnSO_4$, and pure Mn are antiferro-magnetic. Although pure Ni is ferromagnetic, most of nickel compounds are also antiferromagnetic. Since CoC_2 is ferromagnetic and the spin inversion blocking

temperature increases with increasing size of the nanocrystals, other transition metal acetylide compounds are expected to be ferromagnetic. Magnetic properties of the MnC_2 and NiC_2 nanoparticles synthesized at 78 ºC from their metal chloride compounds and CaC_2 were measured with a SQUID magnetometer (Quantum Design MPMS-7S). The synthesis at this temperature produces mostly several nm size crystals that normally limits the spin inversion blocking temperature lower than the room temperature. MnC_2 particles synthesized at 78 ºC are mostly superparamagnetic but only 10% of the products behaved as magnets at room temperature. MnC_2 particles synthesized at 200 ºC are mostly ferromagnetic exhibit the blocking temperature at 320 K.

Figure 1 displays the temperature change of the magnetic susceptibility of NiC_2 under the zero-field cooling (ZFC) condition and the field cooling (FC) at 50 Oe external field. Although the blocking temperature is seen at 10 K, the hysteresis curve at 1.85 K exhibits the cohesive force as large as 1,660 Oe. Annealing of this sample at 300 ºC for 2 hours changes the average size of 10–20 nm and the blocking temperature increases higher than room temperature.

NiC_2 particles are stable at the atmospheric condition, while MnC_2 is damaged by water in the atmosphere. On heating above 250 ºC, NiC_2 shows segregation into metallic nickel and carbon.

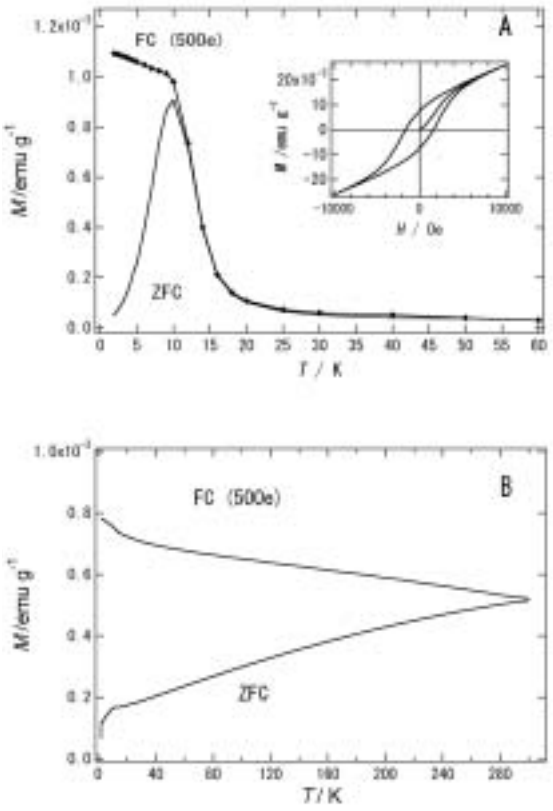

Figure 1. Temperature changes of magnetic susceptibility(*M*) of NiC_2 nanocrystals synthesized at 75 °C (**A**) and measured under the zero-field cooling condition (ZFC) and the field cooling (FC) condition. Inserted in **A** is a magnetic hysteresis curves at 1.8 K. Annealing at 300 °C for 2 hours produced 10 nm-size particles and the *M*-*T* curves change drastically as seen in B.

III-A-4 XAFS and XANES Studies of CoC_2

KOSUGI, Kentaroh; BUSHIRI, Junaid M.; HINO, Kazuyuki; YOKOYAMA, Toshihiko; NISHI, Nobuyuki

$Co^{2+}C_2^{2-}$ nano-clusters are ferromagnetic in contrast with antiferromagnetic electronic structure of $Co^{2+}O^{2-}$. CoC_2 nanoparticles are synthesized from acetonitrile solution of $CoCl_2$ with suspended CaC_2 fine powder. The products obtained from the solution at 340 K is called Sample LT (low temperature product). The CoC_2 nanoparticles are also synthesized from the thermal or photochemical reaction of $Co_4(CO)_{12}$ with solvent CH_2Cl_2. The particles are embedded in amorphous carbon. This sample is called Sample ME (matrix embedded).

XANES: The peak at 7724 eV seen for Sample LT coincides with that of hydrated Co^{2+} ion (as seen for $Co(NO_3)_2(6H_2O)$ suggesting that the Co is in a divalent cation state. The matrix embedded sample (Sample ME) also exhibits the peak at the same energy, while the width is expanded. This is in accord with the appearance of C_2^{2-} infrared absorption bands.

XAFS: The Fourier transform spectrum of XAFS signals of Sample ME exhibited a little difference from that of Sample LT, particularly in the region from 3.2 ~ 4.5 Å. As clearly seen from the appearance of water bands in IR spectra, the two samples contain coordinated water molecules. Therefore the peaks at 1.6 Å (2.08 Å after phase factor correction) are contributed from both Co–C and Co–O pairs. It is very difficult to analyze this peak. The peak at 2.80 Å (3.18 Å after phase factor correction) and other main peaks at much longer distances are attributed to Co–Co pairs. There is little contribution from the direct Co–Co bond at 2.05 Å (2.5 Å after phase factor correction). We have found, however, that the presence of oxygen gas in the solvent results in the appearance of the 2.05 Å peak. The de-oxygenation treatment in a globe box by Ar bubbling longer than 6 hours is necessary . On the basis of the assumption that the Co–C pairs hardly contribute to the peaks at distances longer than 3.5 Å, the Fourier transform spectra of Sample ME are analyzed with the models presented in Figure 1. Most of peaks are reproduced nicely, while the discrepancies in intensities between the calculated and observed spectra become serious at longer distances. This is thought due to the structural disorder in nano-particles. The observed spectra shows drastic intensity decrease at longer distances.

The structure of Sample ME is close to that of MgC_2. The structures derived from the analyses for Sample LT and Sample ME are shown on the top and the bottom of Figure 1.

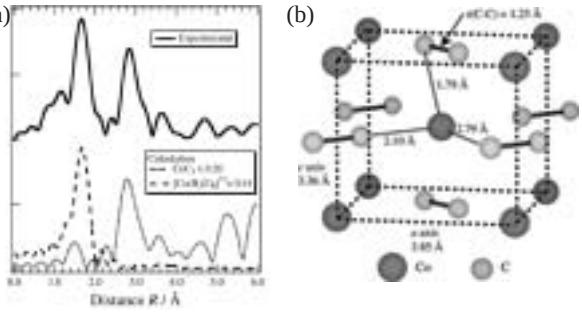

Figure 1. (a) Fourier transform of EXAFS signal. (b) Structure model of CoC_2.

III-A-5 Matrix Embedded Cobalt-Carbon Nano-Cluster Magnets: Behavior as Room Temperature Single Domain Magnets

NISHI, Nobuyuki ;KOSUGI, Kentaroh; HINO, Kazuyuki; YOKOYAMA, Toshihiko

[*Eur. J. Phys. D* **24**, 97 (2003)]

A new type of Co–C nanoparticles is synthesized from CH_2Cl_2 solution of $Co_4(CO)_{12}$ by heating up to 210 ºC in a closed vessel. Transmission electron microscope (TEM) as shown in Figure 1 and electron energy loss spectroscopy (EELS) observation show that the particles are embedded in amorphous carbon and their average size is 12 nm. The radial structure function obtained from the extended X-ray absorption fine structure (EXAFS) of the Co *K*-edge absorption of the Co–C nanoparticles provides a Co–C average distance of 2.08 Å, and the Co–Co distances of 3.18 Å , and 3.9 (±0.2) Å . The particles exhibit the magnetic hysteresis curve with a coercive force of 200 Oe at 20 K and 260 Oe at 300 K. The temperature dependence of the magnetic susceptibility measured under zero-field cooling and 10 Oe field cooling conditions exhibits the behavior characteristic of a set of single magnetic domain nanomagnets in an amorphous carbon matrix.

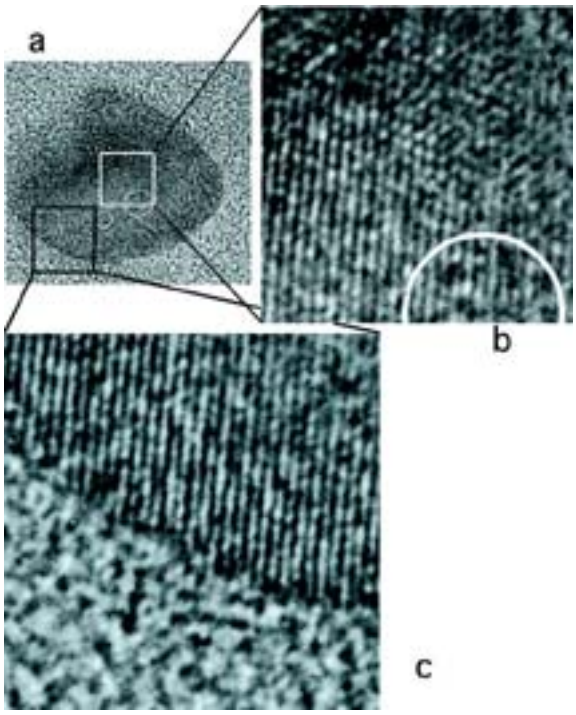

Figure 1. TEM image of a CoC_2 nano-crystal (a). Expanded images (b and c) show tetragonal lattice structure of the crystal.

III-B States of Neutral and Ionic Molecular Associates in Solutions

States of molecular associates particularly in aqueous solutions are of great importance in understanding the role of molecules in living organisms. We found that any ideally mixed state cannot be seen in protic-protic mixtures such as water-alcohol, water-acetic acid, and alcohol-acetic acid systems on the molecular level at solute molar fractions (χ_A) higher than 0.001. In such a system, solute-solute asociation is highly favored resulting in microscopic phase separation. In this year, we studied the aqueous mixture of *N*,*N*-dimethylacetamide (DMA), and have shown that hydrogen bonding between the C=O group and the water molecules and structural changes of predominant solvent clusters were taking place at these specific mole fractions of DMA in aqueous solution.

III-B-1 Structure of Aqueous Mixture of N,N-Dimethylacetamide Studied by Infrared Spectroscopy, X-Ray Diffraction, and Mass Spectrometry

TAKAMUKU, Toshiyuki; MATSUO, Daisuke; TABATA, Masaaki; YAMAGUCHI, Toshio; NISHI, Nobuyuki

[*J. Phys. Chem. B* **107**, 6070 (2003)]

Infrared (IR) spectroscopy and X-ray diffraction measurements have been performed at 298 K on mixtures of *N*,*N*-dimethylacetamide (DMA) and water over the entire range of DMA mole fractions (χ_{DMA}). Mass spectra have also been measured on the clusters that have been isolated by the adiabatic expansion of liquid droplets of the mixtures. The IR overtone band of the C=O stretching vibration for the DMA–D_2O mixtures and the O–D stretching band of HDO for the DMA–H_2O mixtures containing 5% D_2O both shifted to lower frequencies as the water content increased,

accompanied by two inflection points, at χ_{DMA} = 0.1 and 0.6. These results suggested that hydrogen bonding between the C=O group and the water molecules and structural changes of predominant solvent clusters were taking place at these specific mole fractions. The X-ray radial distribution functions have indicated that the structure of the predominant solvent clusters in the mixtures could be classified into four regimes: (1) $0 < \chi_{DMA} \leq 0.1$, where the water clusters predominate; (2) $0.1 < \chi_{DMA} \leq 0.3$, where more water clusters than DMA clusters are formed; (3) $0.3 < \chi_{DMA} \leq 0.6$, where the DMA structure becomes predominant but the water clusters still remain; and (4) $0.6 \leq \chi_{DMA} \leq 1$,where the DMA clusters are dominant in the mixtures. On the basis of the present results on the microscopic structure of the mixtures, the anomalies of thermodynamic parameters such as the enthalpy of mixing are discussed.

III-C Ultrafast Dynamics and Scanning Tunneling Microscopy

For the study of molecules on metallic or crystalline surface, very low temperature Scanning Tunneling Microscope (LT STM) system are now in use for collaboration with users in universities. Ultrafast laser systems with pico and femtosecond time resolutions are also available.

III-C-1 Low Temperature Scanning Tunneling Microscopy for Sub-Nanoscale Systems

WATANABE, Kazuo[3]; OHSHIMO, Keijiro[1]; INOKUCHI, Yoshiya; NAKABAYASHI, Takakazu[2]; NAGATA, Takashi[3]; NISHI, Nobuyuki
([1]RIKEN; [2]Hokkaido Univ.; [3]Univ. Tokyo)

Scanning tunneling microscopy/spectroscopy (STM/STS) is one of the most powerful tools for the real-space observation and the identification of sub-nanoscale materials on the surface. By combining with the ultrashort light pulses, it provides ultimate resolutions of both time and space. Figure 1 shows our STM apparatus which consists of two liquid helium cooled STM heads operating in the ultra-high-vacuum ($\sim 2 \times 10^{-11}$ Torr). The two heads are connected to a sample preparation chamber equipped with an argon ion sputter gun, a gas dosing system, a pulse injection system for the deposition of nanoparticles and bio-molecules, a quadrupole mass spectrometer, and a LEED/AES optics. The STM head (A) is cooled down to 10 K. It has a pair of UV compatible viewing ports from which the sample can be irradiated at ~ 20 K *in situ*. The output pulses (λ = 189 ~ 11200 nm, 4 ps) are introduced through the window from two independently tunable picosecond OPA systems with an optical delay stage. The STM head (B) is cooled below 4 K and used for STS studies. Figure 2 shows an STM image of an Au_{12} cluster (provided by Tsukuda's group) on a graphite surface at 10 K. The size of the cluster is measured ~ 0.8 Å, which is close to the TEM (Transmission Electron Microscope) results. STS investigation of the electronic structures of the nanoclusters is underway. We have also observed the adsorption structure of nitrous oxide molecules on a Pd(110) surface at 10 K (a joint project with Prof. Matsushima's Lab of Hokkaido University).

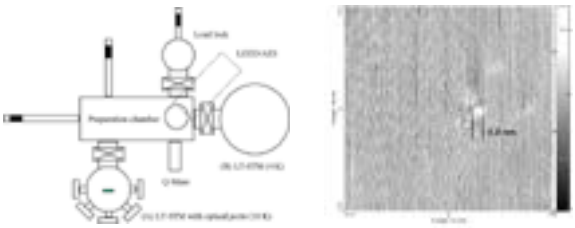

Figure 1. Schematic drawing of the experimental setup.

III-C-2 Ultrafast Time-Resolved Study of *N*-Salicilideneaniline in the Isolated State

OKABE, Chie[1]; NAKABAYASHI, Takakazu[2]; INOKUCHI, Yoshiya; SEKIYA, Hiroshi[1]; NISHI, Nobuyuki
([1]Kyushu Univ.; [2]Hokkaidou Univ.)

N-salicylideneaniline (SA) is a well-known photochromic aromatic anil. The photoexcitation of the $^1(\pi,\pi^*)$ state of the enol form produces the keto form *via* the excited state intramolecular proton transfer (ESIPT). To investigate ultrafast processes in the photoexcited SA, we have applied the femtosecond time-resolved resonance-enhanced multiphoton ionization technique under the isolated conditions. Figure 1 shows the decay profiles of the photoexcited SA measured by the excitation of the enol form with pump wavelength at 320 nm and probe wavelengths at 395 and 790 nm. The time profile in Figure 1 (a) is fitted with three decay components < 230 fs, 1.5 ps, and > 100 ps, while the time profile in Figure 1 (b) is reproduced by the convolution of < 230 fs and 3.5 ps decay components. The < 230 fs decay component is attributed to ultrafast ESIPT from the $^1(\pi,\pi^*)$ state of enol form to the cis-keto form. The 3.5 ps and 1.5 ps decay components are assigned to the ion signal from the $^1(n\pi^*)$ state of the enol form and that the $^1(\pi\pi^*)$ state of the *cis*-keto form produced *via* ESIPT, respectively. We have first to observe the $^1(n\pi^*)$ state of the enol form. The excitation wavelength dependence of ESIPT has been examined in the region from 360 to 373 nm. The rise time of the keto form is less than several hundreds fs even for the

excitation near the red-edge of the absorption of the enol form. In addition, the rise time of the keto form shows no significant OH/OD isotope effect. These results indicate that the ESIPT reaction occurs within several hundreds fs, and the barrier height to ESIPT from the $^1(\pi,\pi^*)$ state is low.

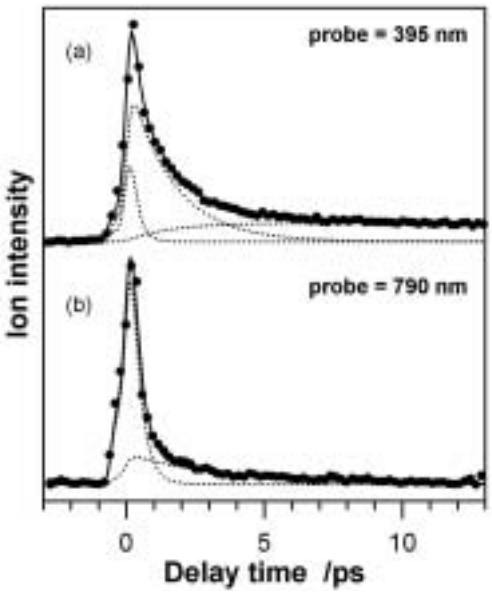

Figure 1. Time evolutions of ion signal of SA detected by femtosecond REMPI with pump wavelength at 320 nm and two different probe wavelengths at 395 nm.

III-C-3 Picosecond Time-Resolved Stokes and Anti-Stokes Raman Studies on the Photochromic Reactions of Diarylethene Derivatives

OKABE, Chie[1]; NAKABAYASHI, Takakazu[2]; FUKAMINATO, Tuyoshi[1]; KAWAI, Tsuyoshi[1]; IRIE, Masahiro[1]; SEKIYA, Hiroshi[1]; NISHI, Nobuyuki
([1]Kyushu Univ.; [2]Hokkaidou Univ.)

[*J. Phys. Chem. A* **107**, 5384 (2003)]

The cyclization and cycloreversion reactions of diarylethene derivatives have been studied with picosecond time-resolved Stokes and anti-Stokes Raman spectroscopies. The cyclization reaction of 1,2-bis(2,5-dimethyl-3-thienyl)perfluorocyclopentene (DMTF) is found to occur within 4 ps to produce the vibrationally excited closed forms in the ground electronic (S_0) state. The time constant of the vibrational relaxation toward a thermal equilibrium with solvent molecules is estimated to be about 10 ps. The cycloreversion reaction of 1,2-bis(3,4-dimethyl-5-phenyl-2-thienyl)perfluorocyclopentene (DMPTF) also generates the vibrationally excited open forms in the S_0 state within 4 ps, which decay on a picosecond time scale. The picosecond time-resolved anti-Stokes Raman spectra of DMPTF show two vibrational bands assignable to the C=C stretching modes of the cyclopentene and thiophene moieties of the generated open forms. The Raman intensity arising from the cyclopentene moiety relative to that from the thiophene moiety becomes smaller with the delay time, indicating that part of the excess energy generated *via* the cycloreversion reaction is localized on the C=C stretching mode of the cyclopentene moiety. This result suggests that the C=C stretching mode of the cyclopentene moiety is one of the promoting or the accepting modes in the cycloreversion reaction.

III-D Spectroscopic and Dynamical Studies of Molecular Cluster Ions

Electron defficiency of molecular cluster cations can attract electron rich groups or atoms exhibiting charge transfer or charge resonance interaction in the clusters. This causes dynamical structural change such as proton transfer or ion-core switching in hot cluster ions or clusters in solution.

III-D-1 Positive Charge Distribution in $(Benzene)_1(toluene)_2^+$ and $(Benzene)_2(toluene)_1^+$ Studied by Photodissociation Spectroscopy

INOKUCHI, Yoshiya; OHASHI, Kazuhiko[1]; SEKIYA, Hiroshi[1]; NISHI, Nobuyuki
([1]Kyushu Univ.)

[*J. Chem. Phys.* **117**, 10648 (2002)]

The positive charge distribution in benzene–toluene hetero-trimer ions is investigated by photodissociation spectroscopy in the near-infrared (6000–14000 cm^{-1}) and infrared (2800–3150 cm^{-1}) regions. The electronic spectra of $(benzene)_1(toluene)_2^+$ and $(benzene)_2(toluene)_1^+$ in the near-infrared region display the strong bands at 9430 and 8330 cm^{-1}, respectively. These bands are ascribed to the charge resonance band; the positive charge is not localized on a single molecule. The vibrational spectrum of $(benzene)_1(toluene\text{-}d_8)_2^+$ shows three distinct bands at 3054, 3084, and 3108 cm^{-1}; these bands are assigned to the CH stretching vibrations of the benzene moiety. The similarity of the spectral features to those of the neutral benzene monomer suggests that the benzene molecule in the $(benzene)_1(toluene)_2^+$ ion has a neutral character. The positive charge is localized on the toluene dimer unit with a structure written as

$(toluene)_2^+\cdots(benzene)_1$. The vibrational spectrum of $(benzene)_2(toluene)_1^+$ bears a resemblance to that of $(benzene)_2^+$. The vibrational spectrum of $(benzene\text{-}d_6)_2(toluene)_1^+$ shows dissimilar features to the spectrum of the neutral toluene monomer, suggesting that a certain amount of the positive charge is carried by the toluene moiety. These results are explained by the charge resonance interaction between $(benzene)_2$ and $(toluene)_1$. A simple perturbation theory is applied for determining the positive charge distribution in $(benzene)_2(toluene)_1^+$. The probability of finding the charge on the $(benzene)_2$ and $(toluene)_1$ moieties is analyzed to be 58 and 42%, respectively.

III-D-2 Infrared Photodissociation Spectroscopy of [Aniline–$(Water)_n$]$^+$ (n = 1–8)

INOKUCHI, Yoshiya; HONKAWA, Yoshiki[1]; OHASHI, Kazuhiko[1]; SEKIYA, Hiroshi[1]; NISHI, Nobuyuki
([1]Kyushu Univ.)

[*J. Phys. Chem. A* **107**, 4230 (2003)]

Infrared photodissociation spectra of [aniline–$(H_2O)_n$]$^+$ (n = 1–8) are measured in the 2700–3800 cm^{-1} region. The spectra are interpreted with the aid of density functional theory calculations. A substantially red-shifted and broadened transition is distinctly observed at 3105 cm^{-1} for the n = 1 ion, and assigned to the stretching vibration of the hydrogen-bonded NH oscillator of the aniline$^+$ moiety. The spectrum of the n = 2 ion demonstrates a large perturbation to both of the NH oscillators, indicating that each NH bond is bound to a water molecule in the most stable structure. For the n = 3 ion, three broad bands exist at 3070, 3230, and 3420 cm^{-1}, and there are two maxima and a weak hump at 3637, 3723, and 3696 cm^{-1}. The calculated spectrum of the 2-1 branch structure resembles the observed one very well. For the n = 4 ion, there exist three strong bands at 2960, 3100, and 3430 cm^{-1}, and a very weak one at 3550 cm^{-1}. The observed spectrum in the 3600–3800 cm^{-1} region is decomposed into four bands at 3640, 3698, 3710, and 3734 cm^{-1}. These bands are originated from the 2-2 branch isomer except for the 3550 and 3710 cm^{-1}bands. These two bands are due to the other isomer that has the five-membered ring. A characteristic transition in the observed spectrum of the n = 5 ion is the 3684 cm^{-1}band, which hardly emerges in the spectra of n = 1–4. This band is assigned to the free OH stretching vibration of the three-coordinated (double-acceptor–single-donor) H_2O, indicating the ring structure. The n = 5 ion has the five-membered ring structure with the fifth water molecule bound to the terminal (double-acceptor) H_2O. The observed spectra of the n = 6–8 ions show features quite different from those of n = 1–5; a very strong and broad band emerges around 3400 cm^{-1}. It is suggested that the n = 6–8 ions have the proton transfer form with some ring structure.

III-D-3 Infrared Spectra and Structures of $(CH_3NH_2)_nH^+$ (n = 1–4). Binding Features of an Excess Proton

MICHI, Takayuki[1]; OHASHI, Kazuhiko[1]; INOKUCHI, Yoshiya; NISHI, Nobuyuki; SEKIYA, Hiroshi[1]
([1]Kyushu Univ.)

[*Chem. Phys. Lett.* **371**, 111 (2003)]

Infrared photodissociation spectra of $CH_3NH_3^+$–**Ar** and $(CH_3NH_2)_nH^+$ with n = 2–4 are measured in the 2600–3500 cm^{-1} region and analyzed with the aid of ab initio calculations. The intensities of the CH-stretching transitions relative to the NH-stretching transitions increase with increasing n, suggesting the change of the binding features of an excess proton in the clusters. Two CH_3NH_2 molecules in $(CH_3NH_2)_2H^+$ equally share the proton. On the other hand, the proton is localized on the central molecule in $(CH_3NH_2)_4H^+$, forming the CH_3-NH_3^+ core solvated by three CH_3NH_2 molecules.

III-D-4 Fermi Resonance Interaction in Hetero-Dimer and Trimer Ions Containing Aniline$^+$

INOKUCHI, Yoshiya; OHSHIMO, Keijiro; OHASHI, Kazuhiko[1]; HONKAWA, Yoshiki[1]; SEKIYA, Hiroshi[1]; NISHI, Nobuyuki
([1]Kyushu Univ.)

[*Chem. Phys. Lett.* **373**, 568 (2003)]

Vibrational spectra of hetero-dimer and trimer ions containing aniline$^+$ are measured by infrared photodissociation spectroscopy. For the dimer ions, the NH_2 bending overtone band gains its intensity through Fermi resonance interaction with the hydrogen-bonded NH stretching fundamental. Unperturbed frequencies of the NH_2 bending overtone are calculated to be in the range of 3255–3276 cm^{-1}, suggesting that the frequency is almost intact upon cluster formation. For the trimer ions, Fermi resonance interaction occurs mainly between the NH_2 bending overtone and the stretching fundamental of the NH oscillator involved in the stronger hydrogen bond.

III-D-5 Infrared Spectra and Structures of Aniline$^+$–Furan and Aniline$^+$–Phenol: Preference between *p*-Type and *s*-Type Hydrogen-Bonded Structures

HONKAWA, Yoshiki[1]; INOKUCHI, Yoshiya; OHASHI, Kazuhiko[1]; NISHI, Nobuyuki; SEKIYA, Hiroshi[1]
([1]Kyushu Univ.)

[*Chem. Phys. Lett.* **376**, 244 (2003)]

Infrared photodissociation spectra of aniline$^+$–M (M = thiophene, furan and phenol) are measured in the 2700–3700 cm^{-1} region and analyzed by density functional theory calculations. Only a structure with a π-type hydrogen bond is found for aniline$^+$–thiophene. Two structural isomers are identified for aniline$^+$–furan and aniline$^+$–phenol, which have either a π-type or a σ-type hydrogen bond, where an amino proton of aniline$^+$ interacts with the π-electrons or the oxygen atom of the

neutral molecules, respectively. The isomer with a σ-type hydrogen bond is more stable for aniline$^+$–phenol, while less stable for aniline$^+$–furan.

III-D-6 Infrared Photodissociation Spectroscopy of Protonated Formic Acid and Acetic Acid Clusters

INOKUCHI, Yoshiya; NISHI, Nobuyuki

[*J. Phys. Chem. A* in press]

Infrared photodissociation spectra of protonated formic acid clusters, $H^+\cdot(HCOOH)_{2-5}$, are measured in the 3000–3700 cm^{-1} region. Density functional theory calculation is applied to $H^+\cdot(HCOOH)_{2-5}$. Geometry optimization of $H^+\cdot(HCOOH)_{2-5}$ indicates that stable forms of these clusters are open chain structures with free OH groups at both ends. In the infrared photodissociation spectra of the n = 2 and 3 species, there are two sharp bands in the range of 3400–3700 cm^{-1}. The lower- and higher-frequency bands of them are attributed to the free OH stretching vibrations of the peripheral COOH groups in the *E* and *Z* conformations, respectively. The intensity of the higher-frequency band relative to that of the lower-frequency one decreases from n = 2 to 3. The n = 4 and 5 ions show only one sharp band in the same region. This band is assigned to the free OH stretching vibrations of the end COOH groups in the *E* conformation; the n = 4 and 5 ions have the peripheral COOH groups only in the *E* conformation. We observe infrared photodissociation spectra of $H^+\cdot(HCOOH)_{6,7}$ in the 3500–3600 cm^{-1} region. The absence of any free OH band for n = 7 shows that both ends of chain structures of n = 7 are terminated by cyclic dimers. Infrared photodissociation spectra of $H^+\cdot(CH_3COOH)_{2-5}$ are also examined in the 3000–3700 cm^{-1} region. Resemblance of the spectra of $H^+\cdot(CH_3COOH)_n$ to those of $H^+\cdot(HCOOH)_n$ suggests that the acetic acid clusters have structures similar to those of the formic acid clusters; the intermolecular network is formed only by the COOH groups.

III-E Spectroscopy and Dynamics of Vibrationally Excited Molecules and Clusters

This research group is studying structure and dynamics of molecules and clusters by two-color double resonance spectroscopy. New spectroscopic methods will also be developed to observe the higher vibrational state under collision-free condition.

A molecular cluster is a microscopic system of solution and/or crystal, and is thought to provide detailed information on relaxation and reaction dynamics in condensed phase. However the previous studies are concentrated to stable clusters which has no reaction pathway after photo-excitation. Consequently, spectroscopic information which concerns the reaction mechanism has not been obtained sufficiently. In this research project started from 2000, we will apply various laser spectroscopies to the reactive clusters to reveal detailed mechanism of intracluster reaction.

For the study of the ground state, the structure of the cluster can be determined by the combination of the IR dip spectroscopy and *ab initio* MO calculations.[1)] The IR dip spectroscopy is a kind of IR-UV double resonance spectroscopy which provides the spectrum which corresponds to the infrared absorption spectrum of the cluster (see Figure 1). A tunable IR laser is introduced to the clusters and is scanned its frequency over the fundamental vibrational region (typically 2400 ~ 4000 cm^{-1}). Then a tunable UV laser, of which the frequency is fixed to the S_1 origin of a specific cluster, is introduced and resonant enhanced multiphoton ionization signal *via* S_1 is monitored. When the IR laser is resonant to a vibrational level of the cluster, the ion signal decreases much because of loss of the population in the vibrational ground state. Thus, the IR absorption spectrum of the cluster can be measured by this depletion spectroscopy. The same spectrum can be obtained when the fluorescence intensity from S_1 is monitored instead of the ion current.

The IR spectrum in the excited state S_1 can also be measured by the depletion spectroscopy, when the UV laser is introduced before the IR laser (the UV-IR fluorescence dip spectroscopy; see Figure 2). The molecule is excited to S_1 by the UV laser, and the fluorescence intensity is monitored as well as the IR dip spectroscopy for S_0. Then the S_1 molecules are further excited to the vibrationally excited level in S_1 by the IR laser. In general, the fluorescence quantum yield decreases in the higher vibronic level. Thus, the total fluorescence intensity decreases when the IR laser frequency is resonant to the vibrational level in S_1.

Similarly, the IR spectrum of the ionic cluster can be measured by the depletion spectroscopy (mass-selected ion dip spectroscopy; see Figure 3). The ionic cluster can be prepared by the multiphoton ionization *via* S_1, and the ion current due to the cation cluster of the specific size can be measured through a mass-filter. When the ionic cluster is vibrationally excited by the IR laser, the cluster is dissociated by the vibrational predissociation. Therefore, the IR transition can be measured by the decrease of the parent cluster. The same spectrum can be obtained by monitoring the enhancement of fragments (mass-selected multiphoton dissociation spectroscopy). In addition to these "dip" spectroscopies, the nonresonant ionization detected IR spectroscopy[2)] and the PFI-ZEKE photoelectron spectroscopy[3)] are also important tool to obtain the spectral information in the cation and the overtone states. Based on these spectroscopic techniques, we have measured the IR spectra of solvated clusters,[4)] such as phenol/ammonia,[5)] naphthol/alcohol,[6)] carbazole/water[7)] and 7-azaindole dimers,[8)] and have discussed the relation among geometrical structure, electronic state and intracluster reactions.

From 2001, we have been developing the new ultrafast time-resolved IR spectroscopy for the reactive clusters. The pico second time-resolved vibrational spectroscopy is one of the ideal way to reveal the reaction mechanism directly. Here, we will demonstrate its usefulness by applying the hydrogen transfer reaction in photoexcited PhOH-

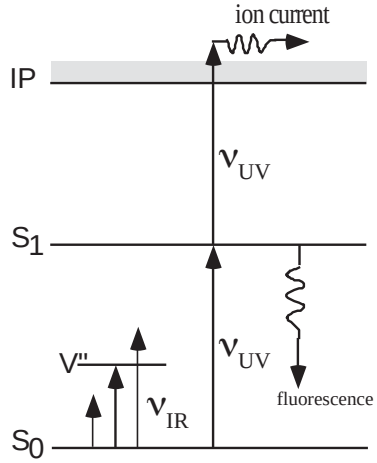

Figure 1. Principle of the IR Dip Spectroscopy. The IR transition in the ground state cluster can be measured.

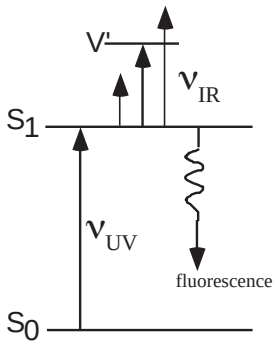

Figure 2. Principle of the UV-IR Fluorescence Dip Spectroscopy. The IR transition of the cluster in the S_1 state can be obtained.

$(NH_3)_n$ cluster.[9] Figure 4 shows the principle of the picosecond time-resolved UV-IR-UV ion dip spectroscopy. The reactive cluster (PhOH-$(NH_3)_n$ in present case) is excited to S_1 by a picosecond UV laser ν_{UV} and the photochemical reaction (hydrogen transfer) is triggered. The final reaction product, *i. e.* $(NH_3)_{n-1}NH_4$, is ionized by a nanosecond UV laser ν_{ION} which is irradiated after 100 ns from ν_{UV} and the population of the reaction product is monitored as a mass peak of $(NH_3)_{n-1}NH_4^+$. A picosecond tunable IR laser ν_{IR} is irradiated after *t* ps from ν_{UV} and is scanned over vibrational region. If ν_{IR} is resonant to vibrational levels of the transient species, the population of the final reaction product decreases due to the vibrational predissociation of the transient species. Therefore, the vibrational transitions of the transient species at t ps can be observed as decrease of ion current of the final reaction product.

Time resolved UV-IR-UV ion dip spectra of phenol-$(NH_3)_3$ are shown in Figure 5. The numbers in the left hand sides of each spectrum indicate the delay time from ν_{UV} to ν_{IR}. Here the spectrum at –20 ns corresponds to the IR spectrum of PhOH-$(NH_3)_3$ in S_0, in which the sharp bands around 3400 cm^{-1}, the broad bands at ~ 3200 cm^{-1} and the very broad background are assigned to the degenerated antisymmetric stretch vibration ν_3 in NH_3, the totally symmetric stretch vibration ν_1 in NH_3 and the OH stretch vibration ν_{OH} in phenol, respectively. The spectrum at + 180 ns shows the vibrational transitions of the final reaction product *via* S_1, *i.e.* $(NH_3)_2NH_4$, and 1) two intense bands at 3180 cm^{-1} and 3250 cm^{-1} and 2) a broad band at 2700 ~ 3100 cm^{-1} which have been assigned to

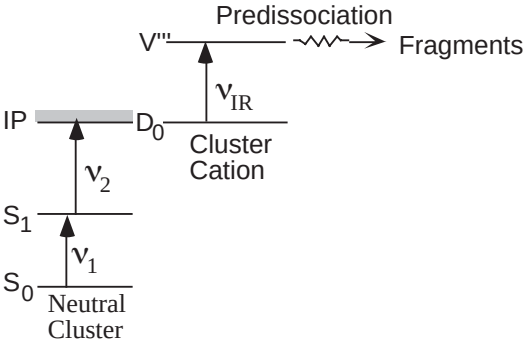

Figure 3. Principle of the mass-selected IR Ion Dip Spectroscopy. The IR transition of the cluster cation can be measured by the depletion of the parent cluster cation. The same spectrum can be measure by monitoring the enhancement of the fragments produced by the IR predissociation.

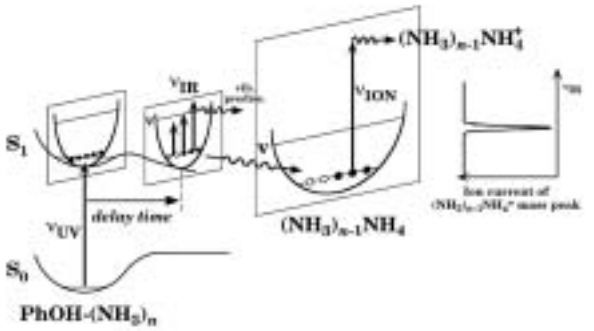

Figure 4. Principle of picosecond time-roselved UV-IR-UV ion dip spectroscopy. Potential curves of S_0 and S_1 are schematically drawn along O–H stretch coordinate. Potential curves in different sections on the S_1 O–H stretch coordinate are drawn along arbitrary N–H stretch coordinates.

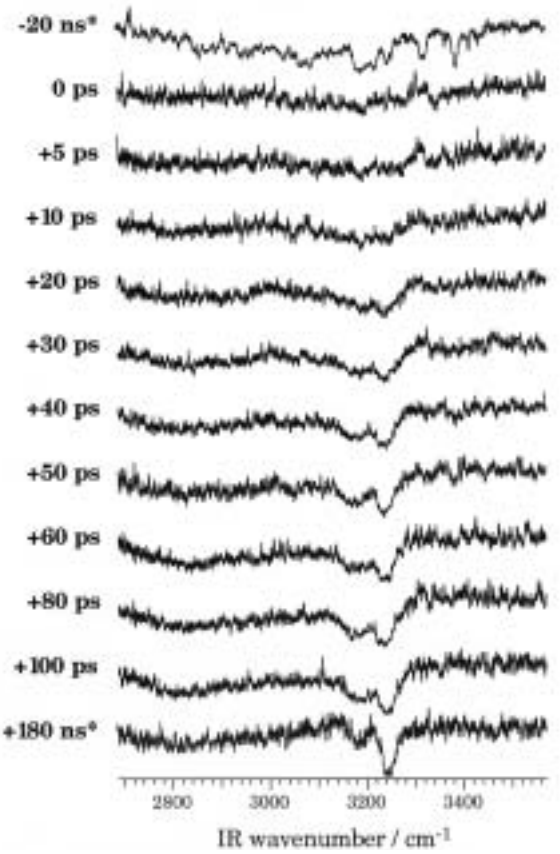

Figure 5. Picosecond time-resolved UV-IR-UV ion dip spectra of the transient species from the electronically excited PhOH-$(NH_3)_3$ which was observed by fixing ν_{UV} to the low vibronic band in the S_1 state of PhOH-$(NH_3)_3$ (281.49 nm) and monitoring $(NH_3)_2NH_4^+$ due to ν_{ION}(355 nm). Times indicated at the left side of each spectrum mean the delay times between ν_{UV} and ν_{IR}. The spectra whose delay times are –20 ns and +180 ns (indicated by *) are obtained by nanosecond laser system, which have been reported in the previous paper.[5]

vibrational transitions concerned with NH_4.

One can see that the vibrational bands rise with increasing delay time. The spectral feature at +100 ps is already similar to that of the final reaction product (+180 ns). Here, the intense band at 3250 cm^{-1} rises slower than the band at 3180 cm^{-1}. The relative intensities of the two bands become comparable at 40 ps, thereafter, the higher band at 3250 cm^{-1} clearly grows further. Thus, the rising time constant of the band at 3250 cm^{-1} is apparently different from that of the 3180 cm^{-1}-band. This remarkable difference between the two intense bands suggests that each vibrational transition is derived from different species. The existence of two transient species are naturally interpreted by considering the isomers of $(NH_3)_2NH_4$; the most stable NH_3–NH_4–NH_3 and the meta-stable NH_4–NH_3–NH_3. The co-existence of isomers is strongly supported by *ab initio* calculations.

As described above, we have successfully measured the picosecond time resolved IR spectra of the transient species for the ESHT of PhOH-$(NH_3)_3$ for the first time. It proves that the picosecond UV-IR-UV ion dip spectroscopy is a powerful tool to explore the dynamics of the intracluster reaction.

References

1) R. Yoshino *et al.*, *J. Phys. Chem. A* **102**, 6227 (1998).
2) T. Omi *et al.*, *Chem. Phys. Lett.* **252**, 287 (1996); S. Ishiuchi *et al.*, *Chem. Phys. Lett.* **283**, 243 (1998).
3) K. Takazawa *et al.*, *Chem. Phys. Lett.* **189**, 592 (1992); K. Müller-Dethlefs *et al.*, *Z. Naturforsch. Teil A* **39**, 1089 (1984); K. Müller-Dethlefs and M. C. R. Cockett, "*Zero Kinetic Energy (ZEKE) Photoelectron Spectroscopy*," Chapter 7, "Nonlinear Spectroscopy for Molecular Structure Determination," R. W. Field *et al.*, Eds., (Blackwell Science, Oxford, 1998), and references therein.; E. W. Schlag, "*ZEKE Spectroscopy*" (Cambridge University Press, Cambridge, 1998) , and references therein.
4) K. Suzuki, Y. Emura, S. Ishiuchi and M. Fujii, *J. Electron Spectrosc.* **108**, 13 (2000), K. Suzuki, S. Ishiuchi and M. Fujii, *Faraday Discuss.* **115**, 229 (2000), K. Sakota, N. Yamamoto, K. Ohashi, H. Sekiya, M. Saeki, S. Ishiuchi, M. Sakai and M. Fujii, *Chem. Phys. Lett.* **341**, 70 (2001).
5) S. Ishiuchi, M. Saeki, M. Sakai and M. Fujii, *Chem. Phys. Lett.* **322**, 27 (2000).
6) M. Saeki, S. Ishiuchi, M. Sakai and M. Fujii, *J. Phys. Chem. A* **105**, 10045 (2001).
7) M. Sakai, K. Daigoku, S. Ishiuchi, M. Saeki, K. Hashimoto and M. Fujii, *J. Phys. Chem. A* **105**, 8651 (2001).
8) H. Yokoyama, H. Watanabe, T. Omi, S. Ishiuchi and M. Fujii, *J. Phys. Chem. A* **105**, 9366 (2001).
9) S. Ishiuchi, M. Sakai, K. Daigoku, T. Ueda, T. Yamanaka, K. Hashimoto and M. Fujii, *Chem. Phys. Lett.* **347**, 87 (2001).

III-E-1 Hydrogen Transfer in Photo-Excited Phenol/Ammonia Clusters by UV-IR-UV Ion Dip Spectroscopy and Ab Initio MO Calculations I: Electronic Transitions

ISHIUCHI, Shun-ichi[1]; DAIGOKU, Kota[2]; SAEKI, Morihisa[3]; SAKAI, Makoto[4]; HASHIMOTO, Kenro[1]; FUJII, Masaaki[4]

([1]Tokyo Inst. Tech./JST-PRESTO; [2]Tokyo Metropolitan Univ./ACT-JST; [3]JAERI; [4]IMS and Tokyo Inst. Tech.)

[*J. Chem. Phys.* **117**, 7077–7082 (2002)]

The electronic spectra of reaction products *via* photo-excited phenol/ammonia clusters (1:2~5) have been measured by UV-near-IR-UV ion dip spectroscopy. Compared with the electronic spectra of hydrogenated ammonia cluster radicals the reaction products have been proven to be $(NH_3)_{n-1}NH_4$ (n = 2 ~ 5), which are generated by excited-state hydrogen transfer in PhOH-$(NH_3)_n$. By comparing the experimental results with *ab initio* molecular orbital calculations at multi-reference single and double excitation CI level, it has been found that the reaction products, $(NH_3)_{n-1}NH_4$ (for n = 3 and 4), contain some isomers.

III-E-2 Hydrogen Transfer in Photo-Excited Phenol/Ammonia Clusters by UV-IR-UV Ion Dip Spectroscopy and Ab Initio MO Calculations II: Vibrational Transitions

ISHIUCHI, Shun-ichi[1]; DAIGOKU, Kota[2]; SAEKI, Morihisa[3]; SAKAI, Makoto[4]; HASHIMOTO, Kenro[1]; FUJII, Masaaki[4]

([1]Tokyo Inst. Tech./JST-PRESTO; [2]Tokyo Metropolitan Univ./ACT-JST; [3]JAERI; [4]IMS and Tokyo Inst. Tech.)

[*J. Chem. Phys.* **117**, 7083–7093 (2002)]

The vibrational spectra of phenol/ammonia clusters (1:2~5) in S_0 and those of their photo chemical reaction products, $(NH_3)_{n-1}NH_4$ (n = 2 ~ 5), which are generated by excited-state hydrogen transfer, have been measured by UV-IR-UV ion dip spectroscopy. The geometries, IR spectra and normal modes of phenol-$(NH_3)_n$ (n = 1 ~ 5) have been examined by *ab initio* molecular orbital calculations, at the second-order Møller-Plesset perturbation theory level with large basis sets. For the n = 2 and 3 reaction products, similar vibrational analyses have been carried out. From the geometrical information of reactants and products, it has been suggested that the reaction products have memories of the reactant's structure, which we call "*memory effect*."

III-E-3 Picosecond Time-Resolved Nonresonant Ionization Detected IR Spectroscopy on 7-Azaindole Dimer

SAKAI, Makoto[1]; ISHIUCHI, Shun-ichi[2]; FUJII, Masaaki[1]

([1]IMS and Tokyo Inst. Tech.; [2]Tokyo Inst. Tech./JST-PRESTO)

[*Eur. J. Phys. D.* **20**, 399–402 (2002)]

The picosecond time-resolved IR spectrum of the 7-

azaindole dimer has been measured by picosecond time-resolved nonresonant ionization detected IR spectroscopy. This new time-resolved technique was developed by combining nonresonant ionization detected IR (NID-IR) spectroscopy with tunable picosecond IR and UV lasers. The time-resolved NID-IR spectrum from 2600 cm^{-1} to 3800 cm^{-1} shows a drastic change from 1.5 ps to 11 ps time evolution. A mode-specific vibrational redistribution has been suggested.

III-E-4 Construction of a Picosecond Time-Resolved IR Dip Spectrometer for Studying Structures and Dynamics of Solvated Clusters

SAKAI, Makoto[1]; UEDA, Tadashi; YAMANAKA, Takaya; FUJII, Masaaki[1]
([1]IMS and Tokyo Inst. Tech.)

[*Bull. Chem. Soc. Jpn.* **76**, 509–514 (2003)]

We have constructed a picosecond time-resolved IR dip spectrometer having a frequency resolution of < 20 cm^{-1} and an instrument response time of 25 ps, respectively. In this system, the second harmonic of the idler wave from the OPA pumped at 800 nm and the remaining light from a regenerative amplifier (< 2.5 mJ/pulse) were differentially mixed in a KTA crystal to generate tunable high-power IR light (2750–4000 cm^{-1}; > 60 μJ). The picosecond time-resolved IR dip spectra of phenol–$(H_2O)_1$ and carbazole–$(H_2O)_1$ are presented to demonstrate the capability of the constructed system. The spectral changes show clear vibrational structures of not only S_0, but also S_1 in the 2800–3800 cm^{-1} energy region. The system performance is also discussed.

III-E-5 Two-Color Far-Field Super-Resolution Microscope Using a Doughnut Beam

WATANABE, Takeshi[1]; IKETAKI, Yoshinori[2]; OMATSU, Takashige[3]; YAMAMOTO, Kimihisa[4]; ISHIUCHI, Shun-ichi[5]; SAKAI, Makoto[1]; FUJII, Masaaki[1]
([1]IMS and Tokyo Inst. Tech.; [2]Olympus Optical Co. Ltd.; [3]Chiba Univ.; [4]Keio Univ./JST-PRESTO)

[*Chem. Phys. Lett.* **371**, 634–639 (2003)]

We have demonstrated a realistic super-resolution scanning fluorescence microscope using conventional nanosecond lasers. This super-resolution microscope is based on the combination of two-color fluorescence dip spectroscopy and shape modulation to a doughnut beam. Only by introducing a doughnut erase beam, the resolution of the laser fluorescence microscope breaks the diffraction limit by two times without using any mechanical probe.

III-E-6 Investigation of the Fluorescence Depletion Process in Condensed Phase

IKETAKI, Yoshinori[1]; WATANABE, Takeshi[2]; ISHIUCHI, Shun-ichi[3]; SAKAI, Makoto[2]; OMATSU, Takashige[4]; YAMAMOTO, Kimihisa[5]; FUJII, Masaaki[2]; WATANABE, Tsutomu[6]
([1]Olympus Optical Co. Ltd.; [2]IMS and Tokyo Inst. Tech.; [3]Tokyo Inst. Tech./JST-PRESTO; [4]Chiba Univ.; [5]Keio Univ.; [6]Univ. Electro-Communications)

[*Chem. Phys. Lett.* **372**, 773–778 (2003)]

By using a two-color dip spectroscopy, we measured the fluorescence intensity from tryptophan in a water solution. The fluorescence intensity exponentially decreased as the laser intensity for the $S_n \leftarrow S_1$ excitation increased. The phenomenon was analyzed by a rate-equation for a three-state model. The analysis shows that tryptophan with the S_n state has a radiationless relaxation process without any process through the S_1 state, and that the $S_n \rightarrow S_1$ internal conversion does not have a 100% yield. The branching ratio of the process is estimated to be 20%. The presented result clarifies in detail the real meaning of Kasha's rule.

III-F Chemical Reaction Dynamics

The research group of Dr. Toshinori Suzuki has moved from IMS to RIKEN (Institute of physical and chemical research) in March 2003.

III-F-1 One- and Two-Color Photoelectron Imaging of the CO Molecule *via* the $B^1\Sigma^+$ State

KATAYANAGI, Hideki; MATSUMOTO, Yoshiteru; DE LANGE, Cornelis A.; TSUBOUCHI, Masaaki; SUZUKI, Toshinori

[*J. Chem. Phys.* **119**, 3737 (2003)]

This paper is concerned with photoelectron imaging following one-color (2+1) and two-color (2+1') resonance enhanced multiphoton ionization (REMPI) in the CO molecule. After the two-photon absorption step $B^1\Sigma^+$ (v' = 0) ←← $X^1\Sigma^+$ (v" = 0) or $B^1\Sigma^+$ (v' = 1) ←← $X^1\Sigma^+$ (v" = 0), the subsequent one-photon ionization $X^2\Sigma^+(v^+)$ ← $B^1\Sigma^+$ (v' = 0,1) shows deviations from the expected Δv = 0 Franck-Condon propensity rule. The results are in good agreement with a previous study using time-of-flight photoelectron spectroscopy (Sha *et al.*, *J. Chem. Phys.* **99**, 4334 (1993)). The experimental photoelectron kinetic energy spectra and their angular distributions are analyzed, and the essential role played by 'superexcited' Rydberg states with an $A^2\Pi$ ion core in this process is examined. Moreover, photoelectron imaging methods appear to be useful in extracting information about superexcited states.

III-G Structure and Properties of Carbon Nanotubes and Nanohorns

We studied growth of single-wall carbon nanotubes (SWNTs) and single-wall carbon nanhorns (SWNHs), and enabled their high-yield and structure-controlled growth. It is shown that the nanometer-scale tubule structures caused the unique behaviors such as one-dimensional fullurene-crystal growth inside SWNTs, size-selective adsorption of gas molecules inside SWNHs, and selective adsoprtion of polypeptides by the oxidized SWNHs. In some application of SWNTs and SWNHs, their immobilization on Si wafers was necessary, which was made possible by using bi-functional molecules with amine at one end and silane at the other end of the linear hydrocarbon molecules. We developed structure analyses methods of carbon nanotubes with electron diffraction analyses with transmission electron microscopy and Raman spectroscopy, and found there is no correlation between the symmetries of inner and outer tubes of double-wall carbon nanotubes.

III-G-1 Causes of Different Catalytic Activities of Metals in Formation of Single-Wall Carbon Nanotubes

YUDASAKA, Masako[1]; KASUYA, Yohko[1]; KOKAI, Fumio[2]; TAKAHASHI, Kunimitsu[3]; TAKIZAWA, Morio[4]; BANDOW, Shunji[5]; IIJIMA, Sumio[1,4,5]
([1]JST; [2]Mie Univ.; [3]IRI; [4]IMS; [5]Meijo Univ.)

[*Appl. Phys. A* **74**, 377–385 (2002)]

When single-wall carbon nanotubes (SWNTs) were formed by pulsed Nd:YAG laser ablation or arc discharge, the yield depended on the metal catalyst: NiCo > Ni ~ NiFe » Co ~ Fe > Pd ~ Pt. It appears that an effective catalyst for SWNT growth must satisfy three conditions: it must be a good graphitization catalyst, have low solubility in carbon, and have a stable crystallographic orientation on graphite. NiCo, Ni, and NiFe satisfy these three conditions. The poor catalytic activities of Co, Fe, Pd, and Pt for SWNT formation would be explained by the ineffectiveness of Pt and Pd as graphitization catalysts, crystallographic orientation instability of Co crystals on graphite, and high solubility of Fe in graphite.

III-G-2 Selective Production of Single-Wall Carbon Nanohorn Aggregates and Their Formation Mechanism

KASUYA, Daisuke[1]; YUDASAKA, Masako[1]; TAKAHASHI, Kunimitsu[2]; KOKAI, Fumio[3]; IIJIMA, Sumio[1,4,5]
([1]JST; [2]IRI; [3]Mie Univ.; [4]IMS; [5]Meijo Univ.)

[*J. Phys. Chem. B* **106**, 4947–4951 (2002)]

Single-wall carbon nanohorn (SWNH) aggregates can be produced by CO_2 laser vaporization of carbon, and a single aggregate can take either a “dahlia-like” or “bud-like” form. We found that “dahlia-like” SWNH aggregates were produced with a yield of 95% when Ar at 760 Torr was used as the buffer gas, while “bud-like” SWNH aggregates were formed with a yield of 70 or 80% when either He or N_2 at 760 Torr was used. The internal structures of both aggregates were studied by partially burning them in an O_2 atmosphere. We were then able to examine the mechanism for the formation of SWNH aggregates.

III-G-3 Fullerene Formation *via* Pyrolysis of Ragged Single-Wall Carbon Nanotubes

KOSHIO, Akira[1]; YUDASAKA, Masako[1]; OZAWA, Masaki[2]; IIJIMA, Sumio[1,3,4]
([1]JST; [2]Univ. Tokyo; [3]IMS; [4]Meijo Univ.)

[*Nano Lett.* **2**, 995–997 (2002)]

A new path of fullerene formation via pyrolysis of ragged single-wall carbon nanotubes (r-SWNTs) which were treated by ultrasonication with an organic solvent followed by heating in oxygen gas is reported. Mass spectrum and high-performance liquid chromatography results indicated that C_{60}, C_{70}, and higher fullerenes existed in products obtained through the pyrolysis of the r-SWNTs at above 800 °C in vacuum. We suggest that the pyrolysis of r-SWNTs originates from holes and defects in the r-SWNTs.

III-G-4 Diameter-Selective Resonant Raman Scattering in Double-Wall Carbon Nanotubes

BANDOW, Shunji[1]; CHEN, Gugang[2]; SUMANASEKERA, Gamini, Udaya[2]; GUPTA, Rajeev[2]; YUDASAKA, Masako[3]; IIJIMA, Sumio[1,3,4]; EKLUND, Peter Clay[2]
([1]Meijo Univ.; [2]Penn. State. Univ.; [3]JST; [4]IMS)

[*Phys. Rev. B* **66**, 075416 (8 pages) (2002)]

Double-wall carbon nanotubes (DWNT’s) have been studied by Raman scattering using different excitation wavelengths and their spectra compared to those of single wall nanotubes (SWNT’s) and C_{60}-SWNT peapods. Raman scattering from the radial and tangential vibrational modes of very small diameter d ~ 0.6–0.9 nm secondary (interior) semiconducting tubes within the DWNT can be unambiguously identified with 647.1 and 1064 nm excitations. The frequency of the tangential displacement vibrational modes identified with these secondary (interior) tubes is found to be downshifted by ~ 7 cm^{-1} relative to that of the larger primary (exterior) tubes that exhibit a diameter d ~ 1.3–1.6 nm. This downshift strongly suggests that at

small tube diameters (*i.e.*, $d \sim 0.7$ nm), the associated wall curvature of the nanotube may require an admixture of sp^3 character in the C–C interaction. Our results also show that the value $\gamma_0 = 2.90$ eV for the nearest C–C tight binding integral is consistent with the resonant enhanced Raman scattering from DWNT's.

III-G-5 Linking Chiral Indices and Transport Properties of Double-Walled Carbon Nanotubes

KOCIAK, Mathieu[1]; SUENAGA, Kazutomo[2]; HIRAHARA, Kaori[1]; SAITO, Yahachi[3]; NAKAHIRA, Takanori[3]; IIJIMA, Sumio[1,4,5]
([1]JST; [2]AIST; [3]Mie Univ.; [4]IMS; [5]Meijo Univ.)

[*Phys. Rev. Lett.* **89**, 155501 (4 pages) (2002)]

We performed *in situ* transport measurement in a transmission-electron microscope (TEM) on individual double-walled carbon nanotubes (DWNT). Using selected-area electron diffraction, the chiral indices of the two tubes constituting the DWNTs were determined through careful comparison with theory. We discuss the case of a DWNT whose two tubes have a gap at half filling and show a finite density of delocalized state at the Fermi level. The exact determination of chiral indices should be reachable in any transport-measurement experiment with samples that allow TEM characterization.

III-G-6 Diameter-Selective Removal of Single-Wall Carbon Nanotubes through Light-Assisted Oxidation

YUDASAKA, Masako[1]; ZHANG, Minfang[1]; IIJIMA, Sumio[1,2,3]
([1]JST; [2]IMS; [3]Meijo Univ.)

[*Chem. Phys. Lett.* **374**, 132–136 (2003)]

When single-wall carbon nanotubes (SWNTs) were treated with H_2O_2, rates of SWNT oxidative-degradation were found to be enhanced with irradiation of light. Raman spectroscopic study indicated that, when the irradiation periods were 2 and 5 min, the radial breathing modes of SWNTs having gap energies corresponding to the wavelength of the irradiated light selectively disappeared. This result suggests that SWNTs having a gap energy corresponding to the wavelength of the irradiated light were preferentially removed.

III-G-7 Single-Wall Nanostructured Carbon for Methane Storage

BEKYAROVA, Elena[1]; MURATA, Katsuyuki[1]; YUDASAKA, Masako[1]; KASUYA, Daisuke[1]; IIJIMA, Sumio[1,2,3]; TANAKA, Hideki[4]; KANOH, Hirofumi[4]; KANEKO, Katsumi[4]
([1]JST; [2]IMS; [3]Meijo Univ.; [4]Chiba Univ.)

[*J. Phys. Chem. B* **107**, 4681–4684 (2003)]

Open single-wall carbon nanohorns (SWNHs) were compressed repeatedly at 50 MPa to generate a nanocarbon material of high bulk density. TEM observations and Raman spectroscopy revealed a significant distortion in the structure of the compressed SWNHs. The obtained nanostructured disordered carbon exhibits a high methane storage capacity, reaching 160 cm^3/cm^3 of nanocarbon at 3.5 MPa and 303 K. Comparison of the experimental results with grand canonical Monte Carlo simulations indicates the importance of the adsorption in the interstitial channels for the high total adsorption capacity of the generated nanostructured carbon.

III-G-8 Nanowindow-Induced Molecular Sieving Effect in a Single-Wall Carbon Nanohorn

MURATA, Katsuyuki[1]; HIRAHARA, Kaori[1]; YUDASAKA, Masako[1]; IIJIMA, Sumio[1,2,3]; KASUYA, Daisuke[1]; KANEKO, Katsumi[4]
([1]JST; [2]IMS; [3]Meijo Univ.; [4]Chiba Univ.)

[*J. Phys. Chem. B* **106**, 12668–12669 (2002)]

Subnanoscale windows (nanowindows) were donated to the walls of single-wall carbon nanohorns (SWNHs) by oxidation in oxygen at different temperatures of 573–693 K. We determined the accessibility of internal nanospaces of the SWNHs through nanowindows to He, Ar, N_2, CH_4, SF_6, and C_{60}. An explicit molecular sieving effect of SWNHs due to the nanowindow was shown.

III-G-9 Binary Nano-Materials Based on Nano-Carbons: A Case for Probing Carbon Nanohorns' Biorecognition Properties

ZHU, Jin[1]; KASE, Daisuke[2]; SHIBA, Kiyotaka[2]; KASUYA, Daisuke[3]; YUDASAKA, Masako[1,3]; IIJIMA, Sumio[1,3,4,5]
([1]JST; [2]Cancer Inst.; [3]NEC; [4]IMS; [5]Meijo Univ.)

[*Nano Lett.* **3**, 1033–1036 (2003)]

A critical step toward the construction of complex architectures based on nanoscale carbonaceous materials is to interface these structures with other useful nanoscale building blocks. Herein we report the synthesis of a new class of binary nanomaterials from single-walled carbon nanohorns and nanoparticles by utilizing a bifunctional molecule as the bridging interconnect. Characterization of the materials by transmission electron microscopy, energy-dispersive X-ray spectroscopy, Raman spectroscopy, and thermogravimetric analysis unambiguously proves the formation of binary nanostructures. The strategy reported here is expected to be generic and readily applicable to carbon nanohorns' interfacing with other nanoscale materials, such as Pt, in the construction of fuel cells. Significantly, with these binary nanomaterials, distinct differences in peptide recognition properties have been identified for carbon nanohorns treated under different conditions through a phage-display enzyme-linked immunosorbent assay. Those peptide recognition motifs are important for exploiting this class of materials in

bioassembly, bioseparation, and biosensing applications.

III-G-10 A Surface Modification Approach to the Patterned Assembly of Single-Walled Carbon Nanomaterials

ZHU, Jin[1]; YUDASAKA, Masako[1,2]; ZHANG, Minfang[1]; KASUYA, Daisuke[2]; IIJIMA, Sumio[1,2,3,4]
([1]JST; [2]NEC; [3]IMS; [4]Meijo Univ.)

A surface modification strategy has been employed for the patterned assembly of single-walled carbon nano-materials onto oxide surfaces. The method relies on distinct molecular recognition properties of different functional groups toward the carbon graphitic structure. The surface modification starts with reactions between bifunctional molecules **1** (with amino and silane groups) and hydroxyl groups on an oxide substrate, generating an amine-covered surface. This is followed by a coupling step where bifunctional molecules **2** (with succinimidyl ester and pyrene groups) react with amines. With one area covered with pyrenyl groups and the other one with hydroxyl groups, patterned assembly of a single layer of single-walled carbon nanohorns (SWNHs) has been demonstrated. The strategy employed, herein, is quite generic and applicable to a variety of oxide substrates, including quartz, SiO_2 layer on Si, and Indium Tin oxide (ITO). Since silane chemistry is compatible with soft or lift-off lithography, an extension of this methodology to micrometer scale patterning has been achieved and a further reduction of the size feature should be possible. In addition, patterned assembly of single-walled carbon nanotubes (SWNTs) has also been realized. These surface immobilized structures should open up new possibilities in such areas as nano-electronics, chemical sensing, field emission displays, nano-tribology, and cell adhesion/bio-recognition investigations.

III-H Wave Packet Engineering Using a Phase-Programmable Femtosecond Optical Source

We proposed "wave packet engineering" which realizes mutual conversion between phase information of photonic and quantum wave packets by means of light-matter interaction. A phase-programmable femtosecond optical source is indispensable for such interactive control of photonic and quantum wave packets. We demonstrate control of quantum wave packets in organic molecules and semiconductors using phase-programmed pulses.

III-H-1 Three-Level Picture for Chirp-Dependent Fluorescence Yields under Femtosecond Optical Pulse Irradiation

HASHIMOTO, Naoyuki T.[1]; MISAWA, Kazuhiko; LANG, Roy[1,2]
([1]CREST(JST); [2]Tokyo Univ. Agric. Tech.)

[*Appl. Phys. Lett.* **82**, 2749–2751 (2003)]

We propose a simple model to account for chirp-dependent fluorescence yields from a substance under femtosecond optical pulse irradiation. The model is simple, consisting of a three-level system, and yet it explains the essential feature of the chirp-dependent fluorescence yields experimentally observed, for example, with cyanine dye molecules. Based on the model, the dependence of the fluorescence on the excitation pulse properties such as the chirp rate and pulse intensity has been examined in detail. The results indicate that chirp-dependent fluorescence can be utilized as a convenient means for characterizing phase distortions in optical pulses such as those in optical fiber communication systems.

III-H-2 Femtosecond Wave Packet Engineering in a Cyanine Dye Molecule

MISAWA, Kazuhiko; MATSUDA, Isao[1]; LANG, Roy[1]
([1]Tokyo Univ. Agric. Tech., CREST(JST))

[*Proc. SPIE–Int. Soc. Opt. Eng.* **4798**, 11–20 (2002)]

Quantum wave packet engineering is demonstrated using a phase-programmable femtosecond optical source. This paper describes development of a programmable phase modulator and coherent control of quantum wave packets. Wave packet motion in a cyanine dye molecule is observed to be dependent on the chirp direction and rate of excitation pulses. Strong reduction in excited state population is efficient for negatively chirped pulses in the cyanine dye molecule, which is explained in terms of a pump-dump process. We discuss a possibility of mutual conversion between the optical and electronic phase information by means of nonlinear light-matter interaction.

III-H-3 Femtosecond Chirp Variable Device Using a Chirped Mirror Pair for Quantum Coherent Control

MATSUDA, Isao[1]; MISAWA, Kazuhiko; LANG, Roy[1]
([1]Tokyo Univ. Agric. Tech., CREST(JST))

[*Appl. Phys. Lett.* submitted]

We demonstrate a femtosecond chirp variable device with a chirped mirror pair to manipulate the chirp rate of pulses precisely. The device is simple, easy-to-use, and compact with high energy durability and low insertion loss. Negative chirp can be added to the pulse digitally without a deviation of the output optical axis, which gives the group velocity dispersion of –42 fs^2 at each reflection on the chirped mirror. The whole device dimension is 180 mm × 76 mm. The reflectively and damage threshold of the chirped mirror are 99.5% and 0.6 J/cm^2, respectively. Using this chirp variable device, a chirp-dependent fluorescence in cyanine dye molecules (IR140) is observed. The device opens a new possibility to manipulate optical phase information.